



Mechanical behaviors of coal surrounding horizontal wellbore during drilling process considering the effects of loading rate, pore pressure and temperature

Qiangui Zhang · Shilin Zhao · Wensong Wang · Xiangyu Fan · Yongchang Liang · Zhigang Jiang · Like Wei · Qiang Yuan

Received: 30 August 2022 / Accepted: 21 November 2022
© The Author(s) 2023

Abstract Coal is a kind of rock with the characteristics of soft structure, developed joints, cleats, cracks, and pores, resulting in that its mechanical behaviors are highly sensitive to stress, pore coalbed methane (CBM, gas) pressure and temperature. Thus, due to the variations in stress, pore pressure and temperature caused by the drilling operation, the coal surrounding wellbore can be easily damaged, which would cause serious wellbore instability problems. In this presented work, a stress path of loading axial stress and unloading confining pressure (LAS-UCP) was first determined based on the stress redistribution of the coal surrounding horizontal wellbore in CBM reservoir during drilling process. A series of

triaxial compression tests with the LAS-UCP stress path was then conducted to study the effects of axial loading rate, pore pressure and temperature on the mechanical behaviors of coal. The results show that: (1) Under the LAS-UCP stress path, the deformation of coal can be divided into elastic deformation stage, plastic deformation stage, and stress reduction stage. With the decrease in axial loading rate and the increases in pore pressure and temperature, the elastic deformation stage becomes shorter, the plastic deformation stage becomes more significant, stress reduction rate in the stress reduction stage becomes slower, and the coal shows more features of plasticity and ductility. (2) With the increasing axial loading

Q. Zhang (✉) · S. Zhao
Petroleum Engineering School, Southwest Petroleum University, Chengdu 610500, Sichuan, China
e-mail: qgzhang@swpu.edu.cn

Q. Zhang · X. Fan
State Key Laboratory of Oil and Gas Reservoir Geology and Exploitation, Southwest Petroleum University, Chengdu 610500, Sichuan, China

Q. Zhang · X. Fan
School of Geoscience and Technology, Southwest Petroleum University, Chengdu 610500, Sichuan, China

W. Wang (✉)
State Key Laboratory of Geohazard Prevention and Geoenvironment Protection, Chengdu University of Technology, Chengdu 610059, Sichuan, China
e-mail: wws@cdu.edu.cn

Y. Liang
Emergency Management Bureau of Emeishan City, Emeishan 614200, Sichuan, China

Z. Jiang
Technical Center, Sichuan Chuanmei Huarong Energy CO.LTD, Chengdu 610091, Sichuan, China

L. Wei · Q. Yuan
State Key Laboratory of Coal Mine Disaster Dynamics and Control, Chongqing University, Chongqing 400044, China

rate, the compressive strength and apparent elastic modulus increase linearly, the absolute values of axial strain, radial strain and volumetric strain at peak stress grow gradually, but the apparent Poisson's ratio changes irregular. (3) With the increase in pore pressure, the compressive strength, axial strain at peak stress and apparent elastic modulus decrease linearly, the radial strain and volumetric strain at peak stress have no change rule, and the apparent Poisson's ratio increases gradually. (4) With the increasing temperature, the compressive strength, axial strain at peak stress and apparent elastic modulus reduce gradually, but the absolute values of radial strain and volumetric strain at peak stress, and the apparent Poisson's ratio increase linearly. The results can not only provide a guidance for safety drilling operation of the horizontal wellbore in CBM reservoir, but also have important significance for other engineering constructions related to coal seam.

Highlights

- LAS-UCP stress path is designed based on stress redistribution of coal around well during drilling.
- Mechanical behavior of coal in LAS-UCP stress path with various axial loading rates is analyzed.
- Mechanical behavior of coal in LAS-UCP stress path with various pore pressures is analyzed.
- Mechanical behavior of coal in LAS-UCP stress path with various temperatures is analyzed.
- Mechanical mechanisms of coal are discussed considering stress path and the three factors.

Keywords Coalbed methane (CBM) · Mechanical behaviors · Unloading confining pressure · Loading rate · Temperature · Pore pressure

1 Introduction

The stability control of wellbore is the most challenging problem in oil and gas development (Tang et al. 2018). Especially, wellbore instability problem is more serious for the drilling operation in Coalbed methane (CBM) reservoir (Li et al. 2018a). This is due to that coal is a kind of rock with the characteristics of soft structure, developed cracks, joints, pores

and cleats (West et al. 2012), resulting in that its mechanical behaviors are highly sensitive to stress (Dutka 2019), pore pressure and temperature (Bhutto et al. 2013; Laouafa et al. 2016). In addition, the stress redistribution and the changes of formation pore pressure and temperature are really significant in the process of drilling operation (Mazaira and Konicek 2015; Miao et al. 2016). Specially, the wellbore instability problem would be more serious for the horizontal wellbore of CBM reservoir due to that the horizontal wellbore would go through much longer than the other types of wellbore considering the horizontal sedimentary characteristics of coal seam. In general, the difference in drilling rate would result in various stress redistribution rate, showing the complex mechanical instability characteristics of multi-factors coupling related to pore pressure and temperature, which has seriously restricted the safe and efficient development of CBM (Jia et al. 2021). Therefore, it is urgently needed to study the mechanical behaviors of coal surrounding horizontal wellbore during drilling process considering the actual engineering situation of stress redistribution rate, variations in pore pressure and temperature.

The instability of horizontal wellbore in CBM reservoir during drilling process is the problem of coal failure under unloading condition. In this process, the stress redistribution will cause multiple loading and unloading on coal, and accelerate the structural damage of coal (Yang et al. 2014; Zhang et al. 2017). In addition, the internal defects of coal, such as joints, cleats, pores and cracks, can easily result in the cracking and damage of coal for the condition of unloading stress, which will also significantly affect the mechanical behaviors of coal (Shen et al. 2020, 2021; Zhou et al. 2020). Thus, lots of works have been done for studying the mechanical behaviors of coal under multiple loading condition. The deformation rate of coal tested under unloading confining pressure (UCP) is much faster than that of coal for conventional triaxial test (Jiang et al. 2017, 2021; Duan et al. 2020). Xin et al. (2018) have found that the stress–strain curve of coal under unloading stress path can be divided into 5 stages: compaction stage, elastic deformation stage, plastic deformation stage, stress reduction stage and residual stress stage. Yin et al. (2013) put forward that the coal elastic modulus would reduce with the increasing confining pressure unloading rate. Wang and Du (2019) proved that the strength of coal tested

under unloading condition is much lower than that of coal tested under conventional triaxial stress condition, as well as, the fracture of coal is affected by multiple stress paths combining with the influence of CBM pressure. Although some valuable works have been done on the mechanical behaviors of coal under UCP condition, few of them focused on the mechanical behaviors of coal surrounding wellbore considering the stress redistribution, coupling the influences of drilling rate, changes of formation pore pressure and temperature, caused by the drilling operation.

The excessive initial gas pressure will make the failure of coal more serious (Xie et al. 2017). Thus, it is necessary to consider the influence of reservoir gas pressure for studying the mechanical behaviors of coal surrounding wellbore in CBM reservoir (Gao et al. 2019). With the increasing gas pressure, the compressive strength, tensile strength and fracture toughness of coal will gradually decrease (Yin et al. 2019), and the compression coefficient will increase (Feng et al. 2021a), as well as, the elastic energy index, impact energy index and dynamic damage time change from strong to weak or none (Ouyang et al. 2020). It has been widely accepted that pore pressure will change the physical–mechanical properties of coal. However, there are few reports on the effect of pore pressure on the mechanical behaviors of coal coupling the stress redistribution condition during drilling CBM reservoir.

Higher temperature will increase the internal energy of gas molecules and form higher pore pressure, leading to obvious changes in mechanical behaviors of coal, and even cause coal failure (Cao et al. 2020). Under a constant confining pressure, a higher temperature would lead to a lower strength of coal (Li et al. 2021a). With the increase in temperature, the elastic modulus and uniaxial compressive strength of coal will reduce, and Poisson's ratio first decreases and then increases (Su et al. 2020). Liu et al. (2019) believed that the increased temperature in coal would lead to pores increase and cracks propagation and increase the coal volume. Gan et al. (2021) found that the average pore diameter, specific surface area and pore volume of coal decrease at first and then increase with the growth of temperature. Most of the above works analyzed the influence of temperature on the physical properties of coal or the mechanical properties of coal only tested under the conventional stress path. There are few studies about the influences

of temperature on the mechanical behaviors coupling the stress redistribution condition during drilling CBM reservoir.

From what have been discussed above, although some studies have been done on the mechanical behaviors of coal considering the influence of UCP and changes of pore pressure and temperature, there are few researches on the mechanical behaviors of coal affected by stress loading rate and the variations in pore pressure and temperature caused by the drilling operation in CBM reservoir. Therefore, considering the stress redistribution of coal surrounding wellbore during the drilling process in CBM reservoir, a series of triaxial mechanical tests was conducted for studying the mechanical behaviors of coal affected by axial loading rate, pore pressure and temperature. The results of our study are of great significance for analyzing the wellbore stability during drilling CBM reservoir.

2 Materials and methods

2.1 Samples

The samples, which were mainly metamorphic coal, were taken from the underground coal seam in Ningwu basin of Shanxi Province, China, as shown in Fig. 1. Ningwu basin is a small structural residual basin in northwest of Shanxi Province, and is mainly developed with Carboniferous Permian coal seams. The coal seams in Ningwu Basin occur at the depth of 300–1500 m (Fan et al. 2016), and the buried depth of these coal seams at both ends and wings of the basin is moderate, showing the excellent CBM accumulation conditions. The samples were collected from the depth of 837 m with the in-situ stress of 16.8–23.5 MPa there. There are many random defects in the coal, resulting in high heterogeneity of it. For reducing the discreteness of experimental results, a relatively complete and uniform coal block was selected for drilling, cutting and grinding, and was made as 15 coal specimens with the size of $\phi 50\text{mm} \times 100\text{ mm}$, as shown in Fig. 1.

2.2 Test scheme

In the process of mining coal seam, the stress of overlying strata in front of the borehole increases at first

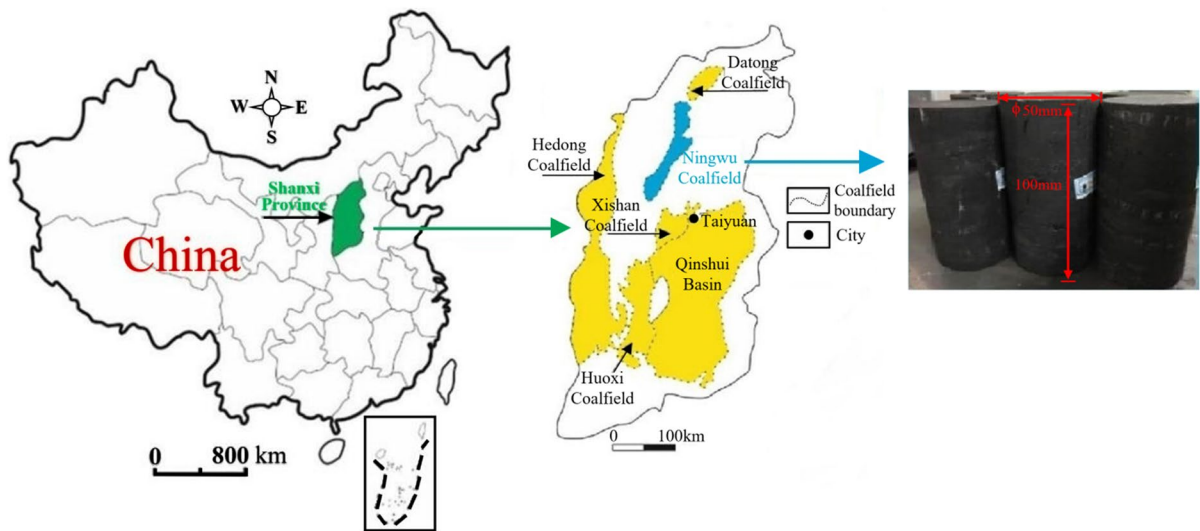


Fig. 1 Geographical location map of Ningwu Coalfield (Liu et al. 2020) and coal specimens

and then decreases, and the horizontal stress increases gradually (Xie et al. 2015). Similarly, the stress redistribution of the formation near the borehole in this process can be drawn as shown in Fig. 2. In addition, considering the optimal drilling azimuth of horizontal well for maintaining the stability of wellbore which is along the maximum horizontal in-situ stress direction (Fan et al. 2014), the experimental stress conditions are designed as follows combining with the in-situ stress distribution of $\sigma_H > \sigma_h > \sigma_v$ in the study area: axial stress (σ_1) is used to simulate the maximum horizontal in-situ stress (σ_H); confining pressure (σ_3) is used to simulate the stress of overlying strata (σ_v). Thus, according to the stress condition as shown in Fig. 2, σ_1 and σ_3 can be drawn from A_0 to A_3 (the coal is assumed to be failure at A_2), as presented in Fig. 3. The stress change from A_1 to A_3 is simulated in this study, which is the stress path of loading axial stress and unloading confining pressure, named as LAS-UCP stress path here, and the initial values of σ_1 and σ_3 at A_1 are set as 20 MPa and 30 MPa, respectively, according to the in-situ stress range of the samples collecting area as mentioned in Sect. 2.1. For the coal seam buried depth, the depth over 800 m is generally defined as the deep formation in China (Xie et al. 2015), and the initial values of σ_1 and σ_3 set here are corresponding to 950 m and 1430 m respectively, calculated by the average rock bulk density of 2.15 g/cm^3 according to the stratigraphic sequences

of overlying rocks in this area (Wang et al. 2015), which are both much deeper than 800 m, indicating that the initial values of σ_1 and σ_3 applied on coal in this study is really high for the sample collecting coal seam. Furthermore, since the fluids exchange between coal seam and wellbore would be prevented by the mud cake on the well wall (Gu et al. 2017), the pore pressure in coal for this study is regarded as a constant value according to the original formation pressure state. Actually, the original formation pressure would be different, and the temperature is also variational considering the original formation condition and the heat exchange between formation and drilling fluid. Therefore, all the experiments are conducted with LAS-UCP stress path, as well as the following three factors are considered: the different axial loading rates caused by variational drilling rate, the different pore pressure and temperature caused by the differences of the original formation condition and the heat exchange. The detailed test schemes for analyzing three factors are introduced as follows.

Triaxial compression tests of LAS-UCP stress path with different loading rates of axial stress (LAS-UCP-LR): According to the difference in drilling rates of CBM horizontal well, the axial loading rate is considered as 0.02 MPa/s, 0.03 MPa/s, 0.04 MPa/s, 0.05 MPa/s, 0.06 MPa/s and 0.07 MPa/s, and the stress path is designed as presented in Fig. 4: Firstly, the axial stress and confining pressure are increased

Fig. 2 Stress redistribution applied on the coal seam near the borehole during drilling process. α is the stress concentration factor caused by different excavation methods; β is the confining pressure growth coefficient; λ is the axial stress growth coefficient; γ is the volume-weight (kN/m^3); κ is the axial compression coefficient; H is the formation depth (m); BHP is the bottom hole pressure (MPa)

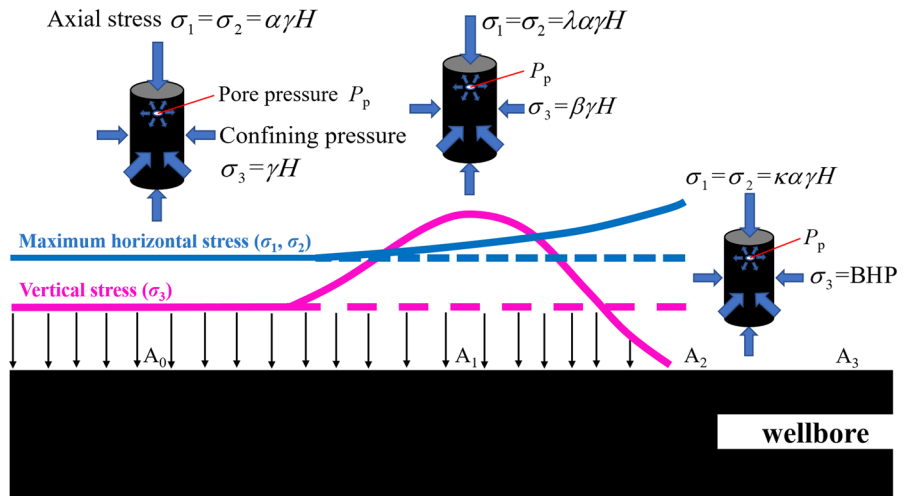


Fig. 3 Stress path design: **a** stress change diagram of the coal surrounding wellbore at the same spatial position during drilling process; **b** stress path of loading axial stress and unloading confining pressure (LAS-UCP stress path)

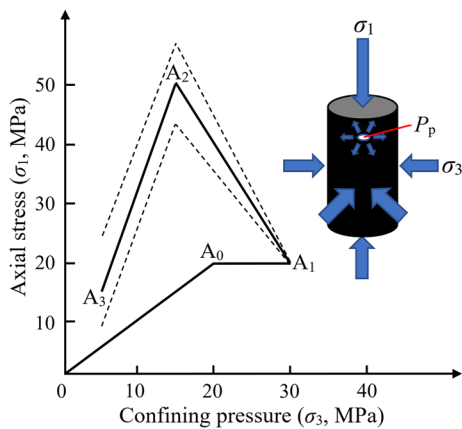
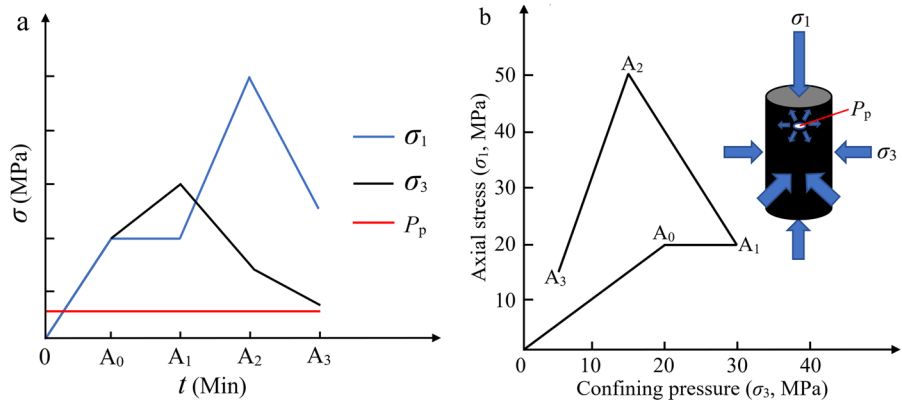


Fig. 4 Stress paths for LAS-UCP-LR tests

to 20 MPa. And then, the axial stress is kept as 20 MPa, and the confining pressure is grown to 30 MPa. Finally, the triaxial compression tests under LAS-UCP stress path with different axial stress loading rate and unloading confining pressure (UCP) rate of 0.01 MPa/s are carried out. The experimental parameters are listed in Table 1.

Triaxial compression tests of LAS-UCP stress path with different pore pressure (LAS-UCP-PP): According to the different reservoir CBM pressure, the constant pore pressures for the triaxial compression tests are set as 1.0 MPa, 2.0 MPa, 3.0 MPa and 4.0 MPa. The experimental parameters are listed in Table 1.

Triaxial compression tests of LAS-UCP stress path with different temperatures (LAS-UCP-T):

Table 1 Experimental parameters of the triaxial compression tests under LAS-UCP stress path

Test scheme	Axial loading rate (MPa/s)	Pore pressure (MPa)	Temperature (°C)	Unloading rate of confining pressure (MPa/s)	Initial axial stress (MPa)	Initial confining pressure (MPa)
LAS-UCP-LR	0.02/0.03/0.04/0.05/0.06/0.07	3.0	24	0.01	20.0	30.0
LAS-UCP-PP	0.04	1.0/2.0/3.0/4.0	24	0.01	20.0	30.0
LAS-UCP-T	0.04	3.0	24.0/33.0/46.0/58.0	0.01	20.0	30.0

According to the differences of reservoir temperature and heat exchange between formation and drilling fluid, the temperatures for the triaxial compression tests are set as 24.0 °C, 33.0 °C, 46.0 °C and 58.0 °C. The experimental parameters are listed in Table 1.

2.3 Experimental apparatus and method

2.3.1 Experiment apparatus

A self-developed apparatus “THM coupling with triaxial servo-controlled seepage apparatus of coal” (Fig. 5) was used for the triaxial compression tests. This apparatus is composed of main frame, pressure chamber, servo loading system, gas pressure control system, constant temperature oil heating system, data acquisition and storage system, and auxiliary system.

2.3.2 Experiment procedure

The triaxial compression tests described in Sect. 2.2 were all conducted as following test procedure: (1) Specimen installation (Zhang et al. 2020): The coal specimen was put between the bottom and top pressure plates. The coal specimen and two pressure plates were then covered by a heat shrinkable tube, and it was heated by a hairdryer to make it closely wrap the coal specimen and the two pressure plates. Next, two metal hoops were used to tighten the heat shrinkable tube at the two pressure plates. Finally, a circumferential extensometer was installed at the coal specimen middle, and an axial extensometer was installed at the both ends of the coal specimen. (2) Initial stress and pore pressure loading (Yin et al. 2015a): an isotropic stress state of $\sigma_1=20$ MPa and $\sigma_3=20$ MPa was applied to the coal specimen, and then confining pressure was increased up to 30 MPa.

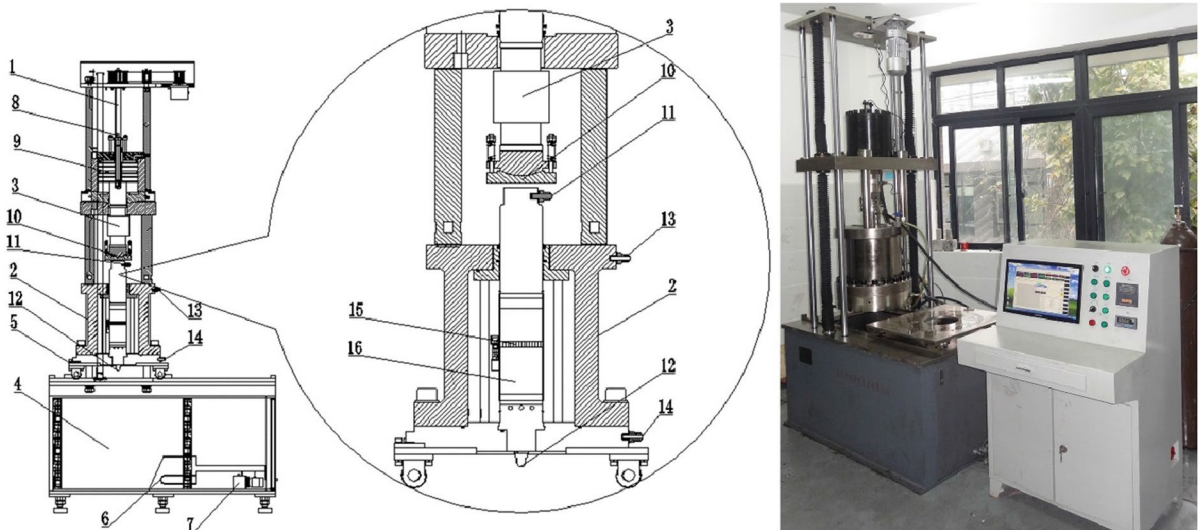


Fig. 5 THM coupling with triaxial servo-controlled seepage apparatus of coal (Li et al. 2016; Yin et al. 2015a). 1-Lifter, 2-Pressure vessel, 3-Sensor of axial stress, 4-Oil tank, 5-Movable work platform, 6-Heater tubes, 7-Oil inlet valve, 8-Sen-

sor of axial displacement, 9-Hydraulic cylinder of axial stress, 10-Force plate, 11-Gas inlet valve, 12-Gas outlet valve, 13-Air drain valve, 14-Hydraulic oil inlet and drain valve, 15-Circumferential extensometers, 16-Specimens

Next, CBM was injected into the coal specimen, and gas outlet valve was closed when the air in the pores was completely replaced by CBM. Following, the pore pressure was kept as the specified value for 12 h to make the coal fully adsorb CBM. (3) Stress loading: the axial stress was loaded with the specified loading rate as shown in Table 1, in the meantime, the confining pressure was unloaded at a rate of 0.01 MPa/s. The axial stress loading was transformed to displacement control with a rate of 0.1 mm/min when the axial stress reached peak value, and the test was ended when only residual stress appeared for the coal specimen.

2.4 Experiment data treatment

Poisson’s ratio (Yin et al. 2015b) and elastic modulus (Cai et al. 2002) are calculated by Eqs. (1) and (2), respectively.

$$\nu = -\frac{d\epsilon_3}{d\epsilon_1} \tag{1}$$

$$E = [\sigma_1 - \nu(\sigma_2 + \sigma_3)] / \epsilon_1 \tag{2}$$

where ν is the Poisson’s ratio, dimensionless; ϵ_3 is the radial strain, %; ϵ_1 is the axial strain, %; E is the elastic modulus, MPa; σ_1 is the axial stress, MPa; σ_3 is the confining pressure, MPa.

The stress–strain relationship for the coal specimens tested under the LAS-UCP stress path may deviate from Hooke’s law due to the complex stress condition of increasing σ_1 and decreasing σ_3 . Thus, the apparent elastic modulus (E_a) and apparent Poisson’s ratio (ν_a) are selected to represent the deformation characteristics of the coal specimens, and the calculation methods of E_a and ν_a are also using Eqs. (1) and (2), respectively.

3 Results and analysis

3.1 Effect of axial loading rate on the mechanical behaviors of coal

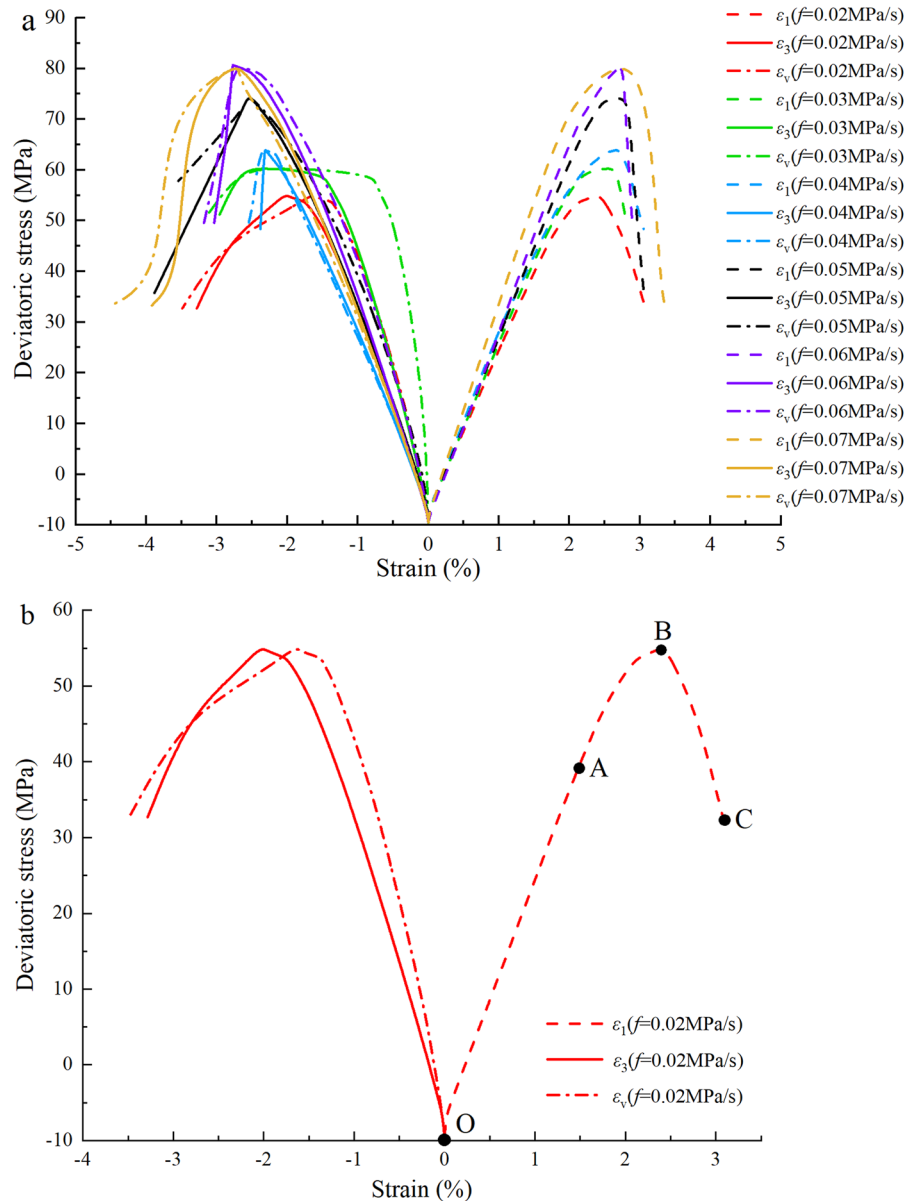
3.1.1 Complete stress–strain curve of the coal specimen for LAS-UCP-LR

Figure 6 presents the complete deviatoric stress ($\sigma_1 - \sigma_3$) versus strains (axial strain ϵ_1 , radial strain ϵ_3

and volumetric strain ϵ_v) curves of the coal specimens tested under different axial loading rates. As shown in Fig. 6, all the coal specimens tested under the LAS-UCP stress path have no obvious compaction stage, this would be caused by the initial stress condition, which is that the initial stresses of σ_1 and σ_3 are high, and the initial σ_3 is greater than the initial σ_1 . Under this initial stress condition, the micro-cracks in the coal specimens would be closed before testing. This matches the actual situation that the coal in front of the wellbore is subjected to an increasing vertical stress and the micro-fractures would be closed gradually, as mentioned in Sect. 2.2. Therefore, these curves are divided into 3 stages (Fig. 6b): (1) Elastic deformation stage (OA section): deviatoric stress grows linearly with the increase of axial strain, and the elastic deformation stage is significant. (2) Plastic deformation stage (AB section): deviatoric stress grows with the increasing axial strain, but the increasing rate reduces gradually. (3) Stress reduction stage (BC section): deviatoric stress reduces rapidly with the increasing axial strain. Although there is a long linear relationship between ϵ_1 and $\sigma_1 - \sigma_3$, the curves of $\sigma_1 - \sigma_3$ versus ϵ_3 and $\sigma_1 - \sigma_3$ versus ϵ_v have a little linear segment due to the effect of UCP (Fig. 6). For example, as shown the result for the coal specimen tested under an axial loading rate of 0.02 MPa/s, the stress difference for the linear segment of the $\sigma_1 - \sigma_3$ and ϵ_1 is 0–40 MPa. However, the stress difference for the linear segment of the $\sigma_1 - \sigma_3$ and ϵ_3 is only 0–5 MPa. The results show that the LAS-UCP stress path will weaken the limitation of the radial deformation, resulting in that the radial deformation is significant and would accelerate with the increase in deviatoric stress.

The stress–strain curves of the coal specimens tested under different axial loading rates show that: (1) The higher the axial loading rate is, the more significant the elastic deformation stage and the shorter the plastic deformation stage will be. For example, the proportions of axial strain increment in the elastic deformation stage to total axial strain before peak stress are 63.66%, 65.11%, 66.60%, 68.38%, 69.67% and 71.21% for the coal specimens tested under the axial loading rates of 0.02 MPa/s, 0.03 MPa/s, 0.04 MPa/s, 0.05 MPa/s, 0.06 MPa/s and 0.07 MPa/s, respectively. (2) The stress reduction rate in the stress reduction stage increases with the increasing axial loading rate. For example, the average stress reduction

Fig. 6 Complete deviatoric stress versus strains curves of the coal specimens: **a** the results of the coal specimens tested under different loading rates; **b**. the typical characteristics of the stress–strain curves. ε_1 is the axial strain, %; ε_3 is the radial strain, %; ε_v is the volumetric strain, %; f is the axial loading rate, MPa



rate in the stress reduction stage is 34.86 MPa/% for the coal specimen tested under an axial loading rate of 0.02 MPa/s, but the average stress reduction rate in the stress reduction stage is 90.13 MPa/% for the coal specimen tested under an axial loading rate of 0.07 MPa/s. These indicate that with the increasing axial loading rate, the elastic-brittle characteristics of coal are enhanced gradually, while the plasticity and ductility characteristics are weakened, this is agreement with the results obtained by Li et al. (2018b).

3.1.2 Strength and strains at peak stress of the coal specimen for LAS-UCP-LR

Figure 7 presents the curves of compressive strength $(\sigma_1 - \sigma_3)_p$ and strains at peak stress (axial strain ε_{1p} , radial strain ε_{3p} and volumetric strain ε_{vp} at peak stress) versus axial loading rates. Figure 7a shows that with the increasing axial loading rate, the compressive strength increases linearly, and the increment of compressive strength is very significant. For

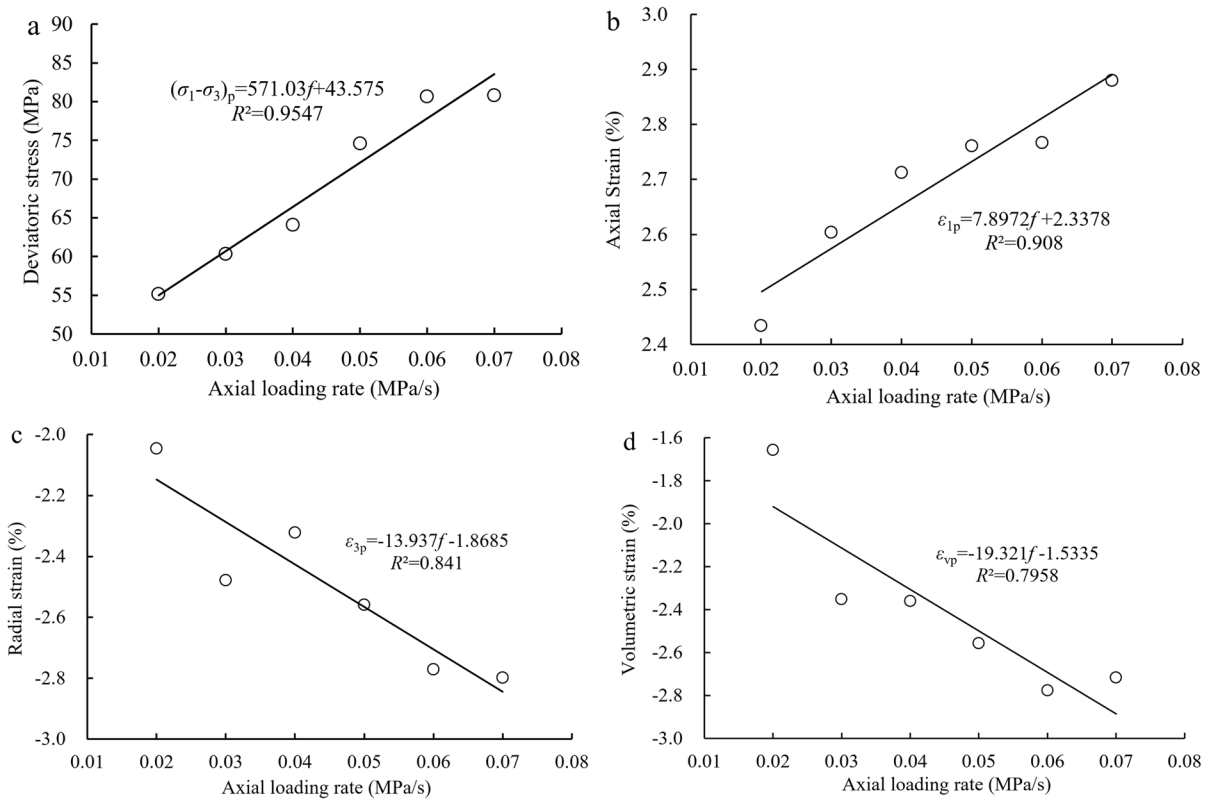


Fig. 7 Curves of compressive strength and strains at peak stress versus axial loading rates: **a** peak deviatoric stress versus axial loading rate; **b** axial strain at peak stress versus axial loading rate; **c** radial strain at peak stress versus axial loading rate; **d** volumetric strain at peak stress versus axial loading

rate. $(\sigma_1 - \sigma_3)_p$ is the peak deviatoric stress; f is the axial loading rate, MPa; ϵ_{1p} is the axial strain at peak stress, %; ϵ_{3p} is the radial strain at peak stress, %; ϵ_{vp} is the volumetric strain at peak stress, %

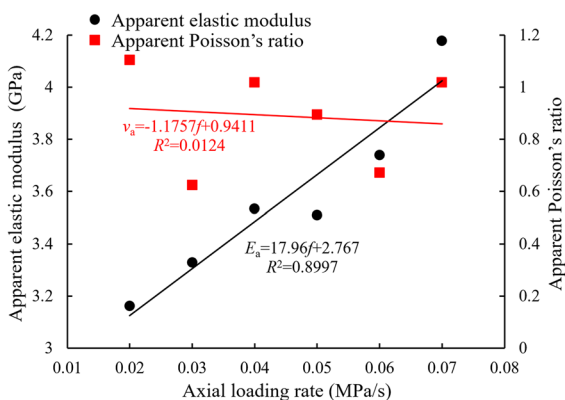
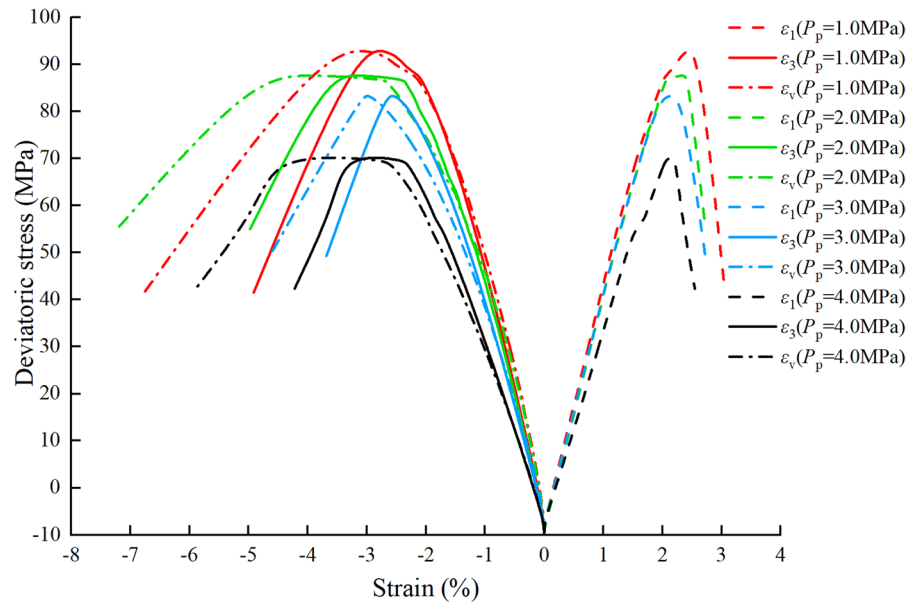


Fig. 8 Curves of apparent elastic modulus (E_a) and apparent Poisson's ratio (ν_a) versus axial loading rate

example, the compressive strength of the coal specimen tested under an axial loading rate of 0.07 MPa/s increases by 46.57% compared with that of the coal specimen tested under an axial loading rate of 0.02 MPa/s. Figure 7b–d show that with the increasing axial loading rate, the ϵ_{1p} and the absolute values of ϵ_{3p} and ϵ_{vp} of the coal specimens increase gradually. In addition, the linear correlation between the ϵ_{1p} and the axial loading rate is better than that between the ϵ_{3p} and the axial loading rate, and the curve of the ϵ_{vp} versus the axial loading rate shows the worst linear correlation. Moreover, the strains at peak stress are significantly affected by the axial loading rate. For example, the ϵ_{1p} , ϵ_{3p} and ϵ_{vp} of the coal specimen tested under an axial loading rate of 0.07 MPa/s

Fig. 9 Complete deviatoric stress versus strains curves of the coal specimens tested under different pore pressures. P_p is the pore pressure, MPa



increase by 18.30%, 36.76% and 63.87%, respectively, compared with those of the coal specimen tested under an axial loading rate of 0.02 MPa/s.

3.1.3 Apparent elastic modulus and apparent Poisson's ratio of the coal specimen for LAS-UCP-LR

Figure 6 shows that it has a significant linear correlation between the $\sigma_1\text{--}\sigma_3$ and ϵ_1 , but the linear segments of the curves for the $\sigma_1\text{--}\sigma_3$ versus ϵ_3 and the $\sigma_1\text{--}\sigma_3$ versus ϵ_v are not obvious. This may be due to that the effect of UCP on the axial deformation can have a hysteresis comparing with the effect of that on the radial deformation (Souley et al.1996). This also implies the reasonability of using apparent elastic modulus (E_a) and apparent Poisson's ratio (ν_a) here. Figure 8 presents the curves of E_a and ν_a versus axial loading rate, which shows that E_a increases approximately in a line with the increasing axial loading rate, indicating that the greater the axial loading rate is, the stronger the elastic accumulation will be (Ma et al. 2021). However, there is a couple of data for the apparent elastic modulus diverging the linear increase trend. For example, E_a of the coal specimen tested under an axial loading rate of 0.04 MPa/s is 3.53 GPa, but the value of the coal specimen tested under an axial loading rate of 0.05 MPa/s is 3.5 GPa, decreasing by 0.85% compared with the former one. This may be due to the heterogeneity of the coal specimens. Figure 8

also shows that ν_a changes irregularly with the increasing axial loading rate, this may due to that the radial deformation of the coal specimen is mainly affected by UCP and the original defects in coal. Especially, the difference of the original defects in coal would lead to a significant difference on radial deformation in the elastic deformation stage. Therefore, the correlation between ν_a and axial loading rate for the coal specimen tested under the LAS-UCP stress path is low.

3.2 Effect of pore pressure on the mechanical behaviors of coal

3.2.1 Complete stress–strain curve of the coal specimen for LAS-UCP-PP

Figure 9 presents the complete deviatoric stress ($\sigma_1\text{--}\sigma_3$) versus strains (ϵ_1 , ϵ_3 and ϵ_v) curves of the coal specimens under different pore pressures tested according to the test scheme of LAS-UCP-PP. Similar to the stress–strain curves of the coal specimens obtained for the LAS-UCP-LR test scheme, the curves presented in Fig. 9 are also divided into the three deformation stages. Moreover, with the increasing pore pressure, the elastic deformation stage decreases significantly, the plastic deformation stage increases observably, and the stress reduction rate in the stress reduction stage decreases gradually. For example, the proportions of the axial strain

increments in the elastic deformation stage to the total axial strains before peak stress are 74.42%, 71.09%, 68.03% and 65.82%, and the average stress reduction rates in the stress reduction stage are 115.47 MPa/%, 90.44 MPa/%, 88.40 MPa/ and 87.58 MPa/ for the coal specimens tested under pore pressures of 1.0 MPa, 2.0 MPa, 3.0 MPa and 4.0 MPa, respectively. Moreover, the curves of deviatoric stress versus strain near the peak stress of the coal specimens tested under various pore pressures have different characteristics: at a low pore pressure, the deviatoric stress changes slowly with the increasing axial strain near peak stress, presenting a "n" shape of their curve; at a high pore pressure, the deviatoric stress changes rapidly with the increasing axial strain near the peak stress, showing a "∧" sharp of their curve. However, at different pore pressure, the deviatoric stress changes slowly with the increases in the radial strain and volumetric strain near the peak stress, showing a "n" shape of their curves. These imply that the pore pressure can affect the failure characteristic of the coal specimen tested under LAS-UCP stress path, showing that the failure characteristic of coal would change from elastic–plastic failure to elastic–brittle failure with the increasing pore pressure.

3.2.2 Strength and strains at peak stress of the coal specimen for LAS-UCP-PP

Figure 10 presents the curves of compressive strength $(\sigma_1 - \sigma_3)_p$ and strains at peak stress (ϵ_{1p} , ϵ_{3p} and ϵ_{vp}) versus pore pressure. As shown in Fig. 10a, the compressive strength decreases approximately in a line with the increasing pore pressure. For example, the compressive strength of the coal specimen tested under a pore pressure of 4.0 MPa decreases by 24.60% compared with that of the coal specimen tested under a pore pressure of 1.0 MPa. From Fig. 10b–d, the following observations can be made: the ϵ_{1p} , the absolute values of ϵ_{3p} and ϵ_{vp} decrease with the increasing pore pressure, indicating that a greater pore pressure would cause a worse deformation capacity of coal, and the coal will be damaged more easily. In addition, the correlation between the three strains at peak stress and the pore pressure is quite different. The regression R-square value (R^2) of the linear fitting between the ϵ_{1p} and the pore pressure is a little lower than 0.9, indicating a good linear correlation between them, while R^2 of the linear fitting between the ϵ_{3p} , ϵ_{vp} and the pore pressure are less

than 0.1. This implies that pore pressure can promote the influence of the original defects of the coal specimen on the radial deformation tested under the LAS-UCP stress path. In this case, the radial deformation at peak stress affected by pore pressure would be more irregular compared with the axial deformation due to the difference in original defects for the different coal specimens.

3.2.3 Apparent elastic modulus and apparent Poisson's ratio of the coal specimen for LAS-UCP-PP

Figure 11 presents the curves of apparent elastic modulus (E_a) and apparent Poisson's ratio (ν_a) versus pore pressure. As shown in Fig. 11, E_a reduces gradually with the increasing pore pressure. For example, the E_a of the coal specimen tested under a pore pressure of 1 MPa is 51.05 GPa, while the E_a of the coal specimen tested under a pore pressure of 4 MPa is 41.46 GPa, decreasing by 18.78% compared with the former one. As shown in Fig. 11, ν_a increases gradually with the increasing pore pressure. For example, the ν_a of the coal specimen tested under a pore pressure of 1 MPa is 0.95, while the ν_a of the coal specimen tested under a pore pressure of 4 MPa is 1.11, increasing by 16.16% compared with the former one.

3.3 Effect of temperature on the mechanical behaviors of coal

3.3.1 Complete stress–strain curve of the coal specimen for LAS-UCP-T

Figure 12 presents the complete deviatoric stress $(\sigma_1 - \sigma_3)$ versus strains (ϵ_1 , ϵ_3 and ϵ_v) curves of the coal specimens tested under different temperatures, showing that the curves also have the three deformation stages. First, with the increasing temperature, the elastic deformation stage decreases, and the plastic deformation stage increases. For example, the proportions of the axial strain increments in the elastic deformation stage to the total axial strains before peak stress of the coal specimens tested under temperatures of 24 °C, 33 °C, 46 °C and 58 °C are 72.62%, 56.08%, 54.97% and 51.60%, respectively. Secondly, in the plastic deformation stage, the higher the temperature is, the more significant the strain growth of the coal specimen within the same deviatoric stress increment

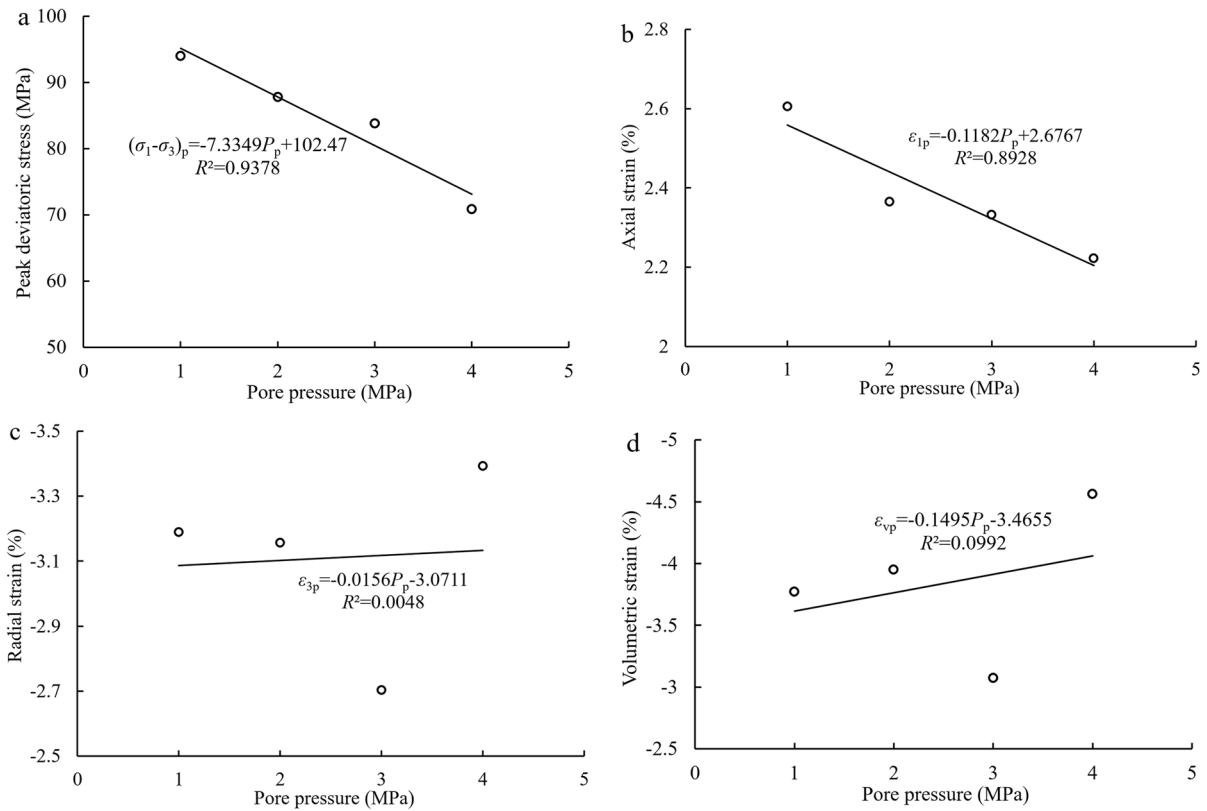


Fig. 10 Curves of compressive strength and strains at peak stress versus pore pressure: **a** peak deviatoric stress versus pore pressure; **b** axial strain at peak stress versus pore pressure; **c**

radial strain at peak stress versus pore pressure; **d** volumetric strain at peak stress versus pore pressure

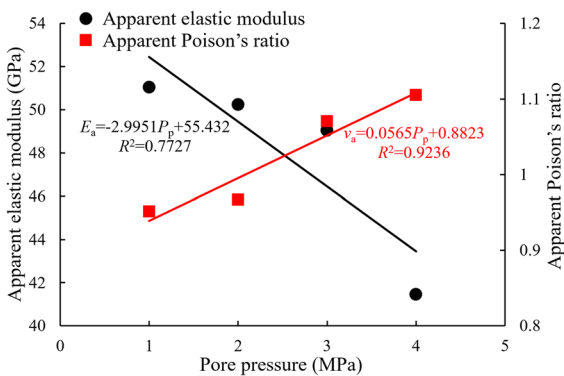
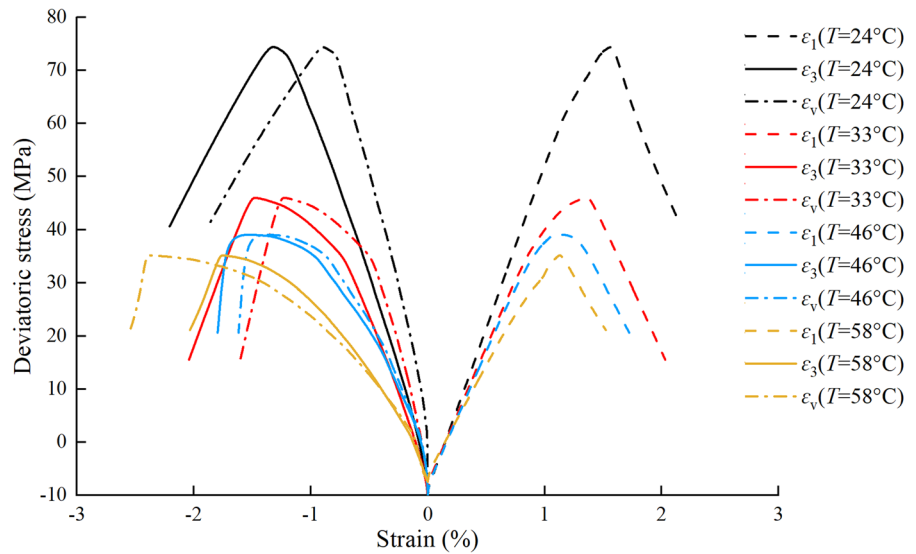


Fig. 11 Curves of apparent elastic modulus (E_a) and apparent Poisson's ratio (ν_a) versus pore pressure

is. For example, when the temperature is 24 °C, deviatoric stress increases by 14.49 MPa while the axial strain increases by 27.38%, that is, the axial

strain in the plastic deformation stage averagely increases by 1.89% for 1 MPa deviatoric stress increase. Correspondingly, when the test temperature is 33 °C, 46 °C and 58 °C, the axial strains in the plastic deformation stage averagely increase by 2.94%, 3.54% and 3.71% for 1 MPa deviatoric stress increase, respectively. Thirdly, the stress reduction rate in the stress reduction stage reduces with the increasing temperature. For example, when the temperature is 24 °C, 33 °C, 46 °C and 58 °C, the average slopes of the stress–strain curves in the stress reduction stage are 56.56 MPa/%, 46.07 MPa/%, 41.28 MPa/% and 38.16 MPa/%, respectively. The above phenomena indicate that the coal specimen tested under the LAS-UCP stress path is more likely to present from the elastic–plastic deformation to plastic or ductile deformation with the increasing temperature.

Fig. 12 Complete deviatoric stress versus strains curves of the coal specimens tested under different temperatures



3.3.2 Strength and strains at peak stress of the coal specimen for LAS-UCP-T

Figure 13 presents the curves of compressive strength $(\sigma_1 - \sigma_3)_p$ and strains at peak stress (ϵ_{1p} , ϵ_{3p} and ϵ_{vp}) versus temperature. As shown in Fig. 13a, the compressive strength decreases gradually and the reduction rate decreases too with the increasing temperature, showing an exponential function relationship between them. For example, the compressive strengths of the coal specimens tested at temperatures of 33 °C, 46 °C and 58 °C decrease by 38.05%, 47.16% and 47.36%, respectively, compared with that of the coal specimen tested at a temperature of 24 °C. This indicates that the increase in temperature will decrease the bond strength of the rock mineral, resulting in a decrease of rock strength (Ersoy et al. 2021). Especially, for the LAS-UCP stress path, the effect of temperature on the decrease of mineral bond strength is more significant than that for the conventional triaxial test (Zhang et al. 2021a), resulting in more serious compressive strength decrease of coal.

From Fig. 13b–d, the following observations can be made: The ϵ_{1p} decreases at an exponential function with the increasing temperature. For example, the ϵ_{1p} of the coal specimens tested at temperatures of 33 °C, 46 °C and 58 °C decrease by 38.05%, 47.16% and 52.64%, respectively, compared with that of the coal specimens tested at a temperature of 24 °C. On the other hand, the absolute values of ϵ_{3p} and ϵ_{vp} increase approximately in a line with the increasing

temperature, showing that the axial deformation capacity would decrease and the radial deformation capacity will increase with the increasing temperature. For example, the ϵ_{3p} of the coal specimens tested at temperatures of 33 °C, 46 °C and 58 °C decrease by 10.68%, 21.97% and 26.15%, respectively, compared with that of the coal specimen tested at a temperature of 24 °C. Accordingly, the ϵ_{vp} decrease by 26.66%, 41.07% and 62.89%. These show that the plasticity and ductility characteristics of coal will become more significant with the increasing temperature, as shown in Fig. 12. However, under the influence of UCP, the ductile deformation of coal mainly reflects in the increase of radial deformation, so even in the case of a small axial deformation, the radial deformation of the coal specimen will also have an obvious value, showing that the ϵ_{1p} decreases gradually, while the absolute values of ϵ_{3p} and ϵ_{vp} increase with the increasing temperature.

3.3.3 Apparent elastic modulus and apparent Poisson’s ratio of the coal specimen for LAS-UCP-T

Figure 14 presents the curves of apparent elastic modulus (E_a) and apparent Poisson’s ratio (ν_a) versus temperature. As shown in Fig. 14, the E_a decreases linearly with the increasing temperature. For example, the E_a of the coal specimens tested at temperatures of 33 °C, 46 °C and 58 °C decrease by 16.04%, 17.68% and 33.62%, respectively, compared with that

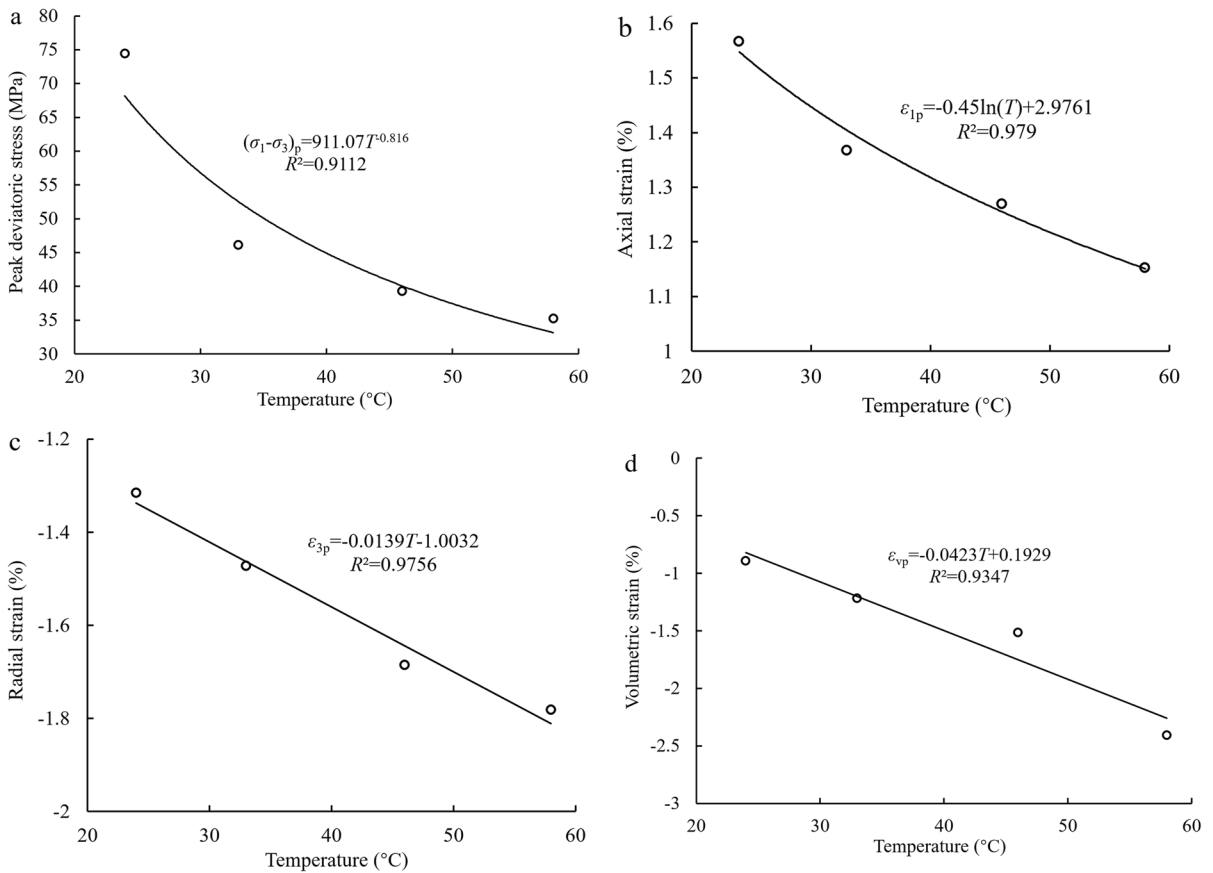


Fig. 13 Curves of compressive strength and strains at peak stress versus temperature: **a** peak deviatoric stress versus temperature; **b** axial strain at peak stress versus temperature; **c**.

radial strain at peak stress versus temperature; **d** volumetric strain at peak stress versus temperature

of the coal specimen tested at a temperature of 24 °C. This implies that the capacity of the coal specimen tested under the LAS-UCP stress path to resist elastic deformation would weaken gradually with the increasing temperature. v_a increases with the increasing temperature, as shown in Fig. 14, showing a good linear relationship between them. For example, the v_a of the coal specimen tested at temperatures of 33 °C, 46 °C and 58 °C increase by 7.28%, 24.99% and 35.54%, respectively, compared with that of the coal specimen tested at a temperature of 24 °C. This implies that the radial deformation of the coal specimen tested under the LAS-UCP stress path would increase linearly with the increasing temperature, resulting in an increase in v_a .

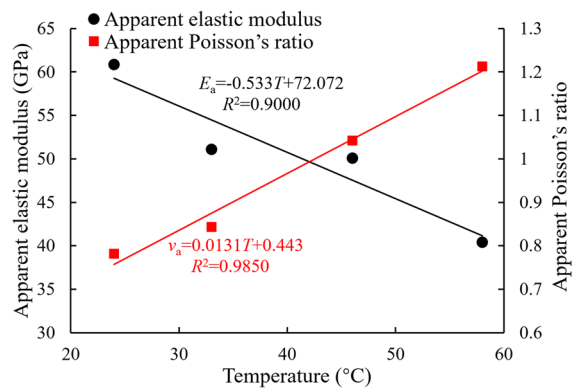


Fig. 14 Curves of apparent elastic modulus (E_a) and apparent Poisson's ratio (v_a) versus temperature. T is the temperature, °C

4 Discussions

The influence mechanism of the LAS-UCP stress path and the three factors can be summarized as the following three points, which are well incorporated into each part of this section: (1) influence of structure defects in coal, including pores, joints, cleats and cracks; (2) gas flow and its effect on the microstructure of rock; (3) influence of water on the mechanical behaviors of coal.

4.1 Influence mechanism of LAS-UCP stress path on mechanical behaviors of coal

Compared with the results for conventional triaxial test (Yang et al. 2007; Zhang et al. 2021a), the plastic deformation of the coal specimen tested under the LAS-UCP stress path accounts for a much shorter proportion to the total deformation before the coal specimen failure; there is even no linear correlation between deviatoric stress and radial strain; as well as, the stress decreases much faster in the stress reduction stage. In addition, the coal specimen tested under the LAS-UCP stress path has lower compressive strength, worse deformation resistance, smaller elastic modulus and larger Poisson's ratio, compared with those obtained by conventional triaxial test (Li et al. 2021b). The reason of the above phenomena would be that the reduction of radial restraint caused by UCP will cause the development and failure of micro-cracks in coal, which thereby significantly weakens the deformation ability of coal, especially in the radial direction, making it more prone to failure (Shen et al. 2021; Zhou et al. 2020). Moreover, the axial loading stress would further promote this failure process, causing a much worse mechanical behaviors of coal under the LAS-UCP stress path compared with that under the conventional triaxial test stress path. The failure of the coal specimen tested under the LAS-UCP stress path mainly depends on inherent defects such as pores, joints, cleats, creaks, growth lines and weak bond zones. From the view of microscopic point, the failure mode of rock subjected to stress is mainly the continuous brittle fracture of locked patches in rock mass (Wei et al. 2022; Wang et al. 2021). According to this failure mode, a faster crack propagation would be obtained for the coal specimen tested under the LAS-UCP stress

path, resulting in poor mechanical behaviors of coal (Kumar et al. 2022).

4.2 Influence mechanism of axial loading rate on mechanical behaviors of coal

The mechanical behaviors of coal affected by the axial loading rate tested under the LAS-UCP stress path can be well explained by the strain energy theory of rock. The internal energy increment per unit time would increase with the increasing axial loading rate. Before the failure of coal, the increased internal energy is mainly transformed into elastic potential energy, plastic potential energy and heat energy, which are stored in coal (Cheng et al. 2021; Feng et al. 2021b; Lu et al. 2022), and these energies can cause the coal to present elastic deformation, plastic deformation, and temperature transformation in coal particles and cement. Actually, these deformations of coal would lag behind the energy concentration, showing that the faster the axial loading rate is, the stronger the accumulation of elastic potential energy in coal will be, and the faster increase of stress will be. It is therefore that the elastic modulus would increase with the increasing axial loading rate (Ma et al. 2021; Guo et al. 2022). Because the radial deformation of coal is sensitive to confining pressure (Feng et al. 2021c), considering the effect of the inevitable nuances in natural defects for the different coal specimens, the radial deformation in the elastic deformation stage of the coal specimen tested under the LAS-UCP stress path changes irregularly with the increasing axial loading rate, as shown in Fig. 6. Thus, the Poisson's ratio has no regularity with the increasing axial loading rate, as shown in Fig. 8. When the coal specimen is damaged, the accumulated potential energy will release rapidly, resulting in a significant stress reduction. And this stress reduction highly depends on the amount of potential energy, and a higher axial loading rate can store more amount of potential energy in coal. Thus, the stress would decrease more rapidly with the increasing axial loading rate, as shown in Fig. 6.

The coal strength is mainly determined by the coal structure and the ratio of stored energy and released energy, expressed as (Duan et al. 2020; Xue et al. 2020):

$$\iota = \frac{\Delta w_c}{\Delta w_f} \quad (3)$$

where ι is the ratio of stored energy and released energy, dimensionless; Δw_c is the energy stored in coal per unit time, J; Δw_f is the released energy of coal per unit time, J. Because the coal specimens used in these tests are taken from one coal block, their structures can be regarded as the same, and the unloading confining pressure (UCP) rates are the same, then the strength is mainly determined by ι . In this case, considering that ι increases linearly with the increasing axial loading rate (Ding et al. 2022), we can therefore infer that the strength would increase linearly, and the axial strain, radial strain, and volumetric strain at peak stress will also increase approximately in a line with the increasing axial loading rate. However, due to the influences of UCP and the inevitable nuances in natural defects for the different coal specimens, especially, the natural defects including pores, joints, cleats, cracks, growth lines and weak bond zones, which have significant impact on rock mechanics behavior (De Silva and Ranjith 2020), the correlations of radial strain and volumetric strain at peak stress versus axial loading rate are relatively poor compared with the correlation between axial strain at peak stress and axial loading rate. As well as, the regularity of the compressive strength and axial strain at peak stress of coal changed with axial loading rate would also be not strictly followed the theoretical rule as mentioned above, as shown in Fig. 7.

4.3 Influence mechanism of pore pressure on mechanical behaviors of coal

The pore pressure mainly produces a tensile stress in coal to promote the radial deformation during the triaxial compression test, and UCP would enhance the effect of pore pressure on the radial deformation. The larger pore pressure would cause lots of tensile cracks in the coal interior (Zhong et al. 2022). Especially, the irreversible tensile fractures would be produced and widened much more seriously in the plastic deformation stage (Wang et al. 2020), improving the permeability of coal (Zou et al. 2021; Cheng et al. 2022). As a result, gas can easily enter into coal and further accelerate the failure process of shear expansion or tension for coal. Therefore, the deformation

of the coal specimen would easier change from elastic deformation to plastic deformation, and the coal specimen would be damaged faster at the stress reduction stage, with the increasing pore pressure. In this case, the elastic deformation stage decreases, the plastic deformation stage increases, and the stress decreases faster in the stress reduction stage, with the increasing pore pressure, as mentioned in Sect. 3.2.1. In addition, the faster deformation in radial direction can also cause a more rapid axial deformation within a unit axial stress increment. So, E_a reduces gradually with the increasing pore pressure (Raziperchikolae et al. 2020), as shown in Fig. 11. Moreover, considering that the effect of pore pressure on the radial deformation of the coal specimen is more significant than the influence of pore pressure on the axial deformation, v_a increases gradually with the increasing pore pressure, as shown in Fig. 11. Furthermore, the increase in pore pressure will cause more gas molecules to be adsorbed on the surface of coal particles (Yin et al. 2012), which would cause coal swelling, further destroy the compactness of coal and accelerate the shear failure and tensile failure of coal. Ultimately, the strength and axial strain at peak stress will reduce with the increasing pore pressure (Hu et al. 2018). These agree with the results of the coal specimens tested under other stress path with unloading confining pressure for different pore pressures (Yin et al. 2015b).

4.4 Influence mechanism of temperature on mechanical behaviors of coal

The influence mechanism of temperature on mechanical behaviors of coal can be summarized as the effect of temperature on coal matrix, pore gas and pore water. The effect on coal matrix: With the increase in temperature, changes such as mineral expansion, mineral decomposition, metallic bond fracture, and even minerals melting will occur in coal, leading to more severe damage to the microstructure of coal matrix. The microstructure variation will cause macro defects in coal, which will lead to the deformation properties of coal from elasticity to plasticity or ductility (Zhang et al. 2022), which makes it quickly reach the critical point of failure. As a result, the mechanical behaviors of coal would sharply decline with the increase in temperature (Su

et al. 2020). In addition, the heterogeneity of coal is very prominent (Hu et al. 2022), the increase in temperature will lead to stress concentration in coal, so it will accelerate the local failure of coal in the testing process. The effect on pore gas: The molecular thermal movement of the coalbed methane (CBM, gas) in the pores of the coal specimen will accelerate with the increasing temperature, resulting in that an uneven expansion of CBM (the gas expansion in large pores is significant, while that in small pores is relatively insignificant), presenting as the increase of pore pressure. This increase of pore pressure will cause extension and extrusion damages to the coal specimen skeleton. Meanwhile, the non-uniform expansion of CBM will make gas molecules form a complex movement and impact the coal skeleton particles, which is more likely to cause instability in the coal skeleton structure tested under the LAS-UCP stress path. The effect on pore water: The coal specimens used in our study are prepared from the natural coal block, there is a little free water and bound water in the coal. As well know, the performance of water in rock is highly affected by temperature, showing that the free water in rock will be released, the bound water, crystal water and structural water will escape from rock particles to form free water with the increase of temperature. In this case, some new micropores and microcracks would appear and the minerals compositions will also change, resulting in the changes of internal structure and chemical and physical characteristics of coal. This has a significant negative impact on coal mechanical behaviors (Zhang et al. 2021b). In general, due to the change of the three aspects affected by temperature as discussed above, the compressive strength, axial strain at peak stress and E_a would decrease, the absolute values of radial strain and volumetric strain at peak stress, and v_a will increase with the increasing temperature, as a result, the coal would show poor mechanical behaviors.

4.5 Implication on the engineering practice

As mentioned in Sect. 2, the LAS-UCP stress path and the three analytical factors, which are designed according to the real situation of the horizontal wellbore drilling process in CBM reservoir, are strictly conducted in these triaxial compression tests. Thus, the mechanical behaviors of the coal specimens can

reflect the properties of the coal surrounding the horizontal wellbore during drilling process. Based on the results as presented in Sect. 3, the following recommendations can be drawn for guiding the drilling operation of the horizontal wellbore in CBM reservoir: (1) A high drilling rate is recommended for drilling the horizontal wellbore in CBM reservoir. But, as time goes on, the stress redistribution would also cause a damage of the coal surrounding the wellbore, thus, the well cementing operation should be done timely to guarantee the stability of the wellbore if the coal surrounding the wellbore has poor mechanical properties. (2) The underbalanced drilling technology is suggested for drilling the horizontal wellbore in CBM reservoir, to let the gas flowing from formation to borehole, with the purpose of decreasing the pore pressure in coal seam. However, the bottom hole pressure must be designed scientifically and be controlled strictly to maintain the wellbore stability. (3) The flow velocity of drilling fluid should be increased and the drilling fluid is recommended to be cooled before returning to the formation, thus, the heat would be carried out by the drilling fluid to reduce the temperature of the coal surrounding the wellbore.

The implication of the results obtained in this paper on the drilling engineering in coal seam is just a simple case to demonstrate the significance of our study. Actually, there are many other engineering constructions related to the coal seam, such as coal mining, tunnel excavation, slope engineering, etc., which have the same situation of the CBM reservoir drilling engineering. The results of this paper can also give an important reference for these engineering constructions related coal seam. Water has not been considered in these tests due to that the mud cake would prevent water in drilling fluid from entering into the formation according to the actual engineering condition of drilling operation. However, water is an important factor to impact the mechanical behaviors of coal for the other engineering constructions (Zou et al. 2022; Liu and Liu 2022; Zhang et al. 2021c), because these engineering constructions should use water for cooling or the surface water would enter into coal seam. Therefore, coupling the effects of the LAS-UCP stress path and water on the mechanical behaviors of coal should be further studied to reveal the physical and chemical influence mechanism of them.

5 Conclusions

According to the stress redistribution of the coal surrounding horizontal wellbore during drilling process, a series of triaxial compression tests was carried out to study the influence of axial loading rate, coal-bed methane (CBM, gas) pore pressure and temperature on the mechanical behaviors of coal. The conclusions can be drawn as follows:

- (1) There is no obvious compaction stage of the coal specimens tested under the LAS-UCP stress path with different axial loading rates, pore pressures and temperatures. The entire deformation process can be divided into elastic deformation stage, plastic deformation stage and stress reduction stage. The radial deformation is significant for the whole deformation process and would accelerate with the increasing deviatoric stress.
- (2) With the increasing axial loading rate, the elastic deformation stage becomes more significant, the plastic deformation stage becomes shorter, the stress reduction rate in the stress reduction stage increases, and the compressive strength increases linearly. The axial strain, the absolute values of radial strain and volumetric strain at peak stress increase gradually, and the apparent elastic modulus (E_a) increases linearly with the increase of axial loading rate, however, the apparent Poisson's ratio (ν_a) shows an irregular change.
- (3) With the increasing pore pressure, the elastic deformation stage decreases significantly, the plastic deformation stage increases observably, and the stress reduction stage decreases slightly. The compressive strength and axial strain at peak stress decrease linearly, and the radial strain and volumetric strain at peak stress have no change rule, the E_a decreases gradually, while the ν_a increases, with the increasing pore pressure.
- (4) With the increasing temperature, the elastic deformation stage decreases, and the plastic deformation stage increases, and the stress reduction rate in the stress reduction stage decreases. The compressive strength, axial strain at peak stress, the E_a decrease linearly with the increasing temperature, but the absolute values of radial strain and volumetric strain at peak stress and the ν_a would increase.

Acknowledgements The financial supports from the Natural Science Foundation of Sichuan Province (Grant No. 2022NSFSC0185) and the National Natural Science Foundation of China (Grant Nos. 42172313 and 51774246) are appreciated. The authors would like to express their gratitude to the editors and anonymous reviewers for their constructive comments on the draft paper.

Author contributions Conceptualization: QZ, XF; methodology: QZ, WW; resources: QZ; formal analysis and investigation: SZ, YL, LW, QY; writing—original draft preparation: QZ, SZ; writing—review and editing: QZ, WW; visualization: YL, ZJ; validation: SZ, LW, QY; funding acquisition: QZ, XF; supervision: WW, XF; project administration: QZ. All authors read and approved the final manuscript.

Availability of data and materials The data used to support the findings of this study are available from the corresponding author upon request.

Code availability Not applicable.

Declarations

Competing interests The authors declare that they have no known competing financial interests or personal relationships that could have appeared to influence the work reported in this paper. The authors declare the following financial interests/personal relationships which may be considered as potential competing interests.

Open Access This article is licensed under a Creative Commons Attribution 4.0 International License, which permits use, sharing, adaptation, distribution and reproduction in any medium or format, as long as you give appropriate credit to the original author(s) and the source, provide a link to the Creative Commons licence, and indicate if changes were made. The images or other third party material in this article are included in the article's Creative Commons licence, unless indicated otherwise in a credit line to the material. If material is not included in the article's Creative Commons licence and your intended use is not permitted by statutory regulation or exceeds the permitted use, you will need to obtain permission directly from the copyright holder. To view a copy of this licence, visit <http://creativecommons.org/licenses/by/4.0/>.

References

- Bhutto AW, Bazmi AA, Zahedi G (2013) Underground coal gasification: from fundamentals to applications. *Prog Energy Combust Sci* 39(1):189–214. <https://doi.org/10.1016/j.peccs.2012.09.004>
- Cai M, He M, Liu D (2002) *Rock mechanics and Engineering*. Science Press, Beijing, pp 26–28 (in Chinese)

- Cao Y, Chen W, Yuan Y, Wang T, Sun J, Cai Y (2020) Experimental study of coalbed methane thermal recovery. *Energy Sci Eng* 8(5):1857–1867. <https://doi.org/10.1002/ese3.637>
- Cheng H, Zhang Y, Zhou X (2021) Nonlinear creep model for rocks considering damage evolution based on the modified Nishihara model. *Int J Geomech* 21(8):1–12. [https://doi.org/10.1061/\(ASCE\)GM.1943-5622.0002071](https://doi.org/10.1061/(ASCE)GM.1943-5622.0002071)
- Cheng X, Luan H, Chen L, Zhang J, Jiang Y (2022) Impact of coal damage on permeability evolution based on an improved permeability model. *J Nat Gas Sci Eng* 101:104509. <https://doi.org/10.1016/j.jngse.2022.104509>
- De Silva VRS, Ranjith PG (2020) A study of rock joint influence on rock fracturing using a static fracture stimulation method. *J Mech Phys Solids* 137:103817. <https://doi.org/10.1016/j.jmps.2019.103817>
- Ding Z, Jia J, Tang Q, Li X (2022) Mechanical properties and energy damage evolution characteristics of coal under cyclic loading and unloading. *Rock Mech Rock Eng* 55:4765–4781. <https://doi.org/10.1007/s00603-022-02884-x>
- Duan M, Jiang C, Xing H, Zhang D, Peng K, Zhang W (2020) Study on damage of coal based on permeability and load–unload response ratio under tiered cyclic loading. *Arab J Geosci* 13:250. <https://doi.org/10.1007/s12517-020-5249-4>
- Dutka B (2019) CO₂ and CH₄ sorption properties of granular coal briquettes under in-situ states. *Fuel* 247:228–236. <https://doi.org/10.1016/j.fuel.2019.03.037>
- Ersoy H, Karahan M, Kolaylı H, Sünnetci MO (2021) Influence of mineralogical and micro-structural changes on the physical and strength properties of post-thermal-treatment clayey rocks. *Rock Mech Rock Eng* 54(2):679–694. <https://doi.org/10.1007/s00603-020-02282-1>
- Fan X, Wu H, Yin S, Xia H, Chen P, Lei M, Qin Y (2014) An optimal method of horizontal interval azimuth for a shale gas well considering wellbore stability and stimulation effects. *Nat Gas Ind* 34(12):94–99. <https://doi.org/10.3787/j.issn.1000-0976.2014.12.013>. (in Chinese)
- Fan F, Zheng Y, Lyu H (2016) Study on coalbed methane reservoir sensitivity in Ningwu Basin and drill-in fluid technology. *Drill Fluid Complet Fluid* 33(1):48–51. <https://doi.org/10.3969/j.issn.1001-5620.2016.01.010>. (in Chinese)
- Feng K, Wang K, Zhang D, Yang Y (2021a) Experimental study on the deformation and permeability characteristics of raw coal under the coupling effect of confining pressure and pore pressure. *Adv Mater Sci Eng* 2021:9983975. <https://doi.org/10.1155/2021/9983975>
- Feng K, Wang K, Zhang D, Yang Y (2021c) Experimental study on mechanical properties and seepage laws of raw coal under variable loading and unloading rates. *Geofluids* 2021:5596858. <https://doi.org/10.1155/2021/5596858>
- Feng Y, Yang X, Liu J, Chen Z (2021b) A new fractional Nishihara-type model with creep damage considering thermal effect. *Eng Fract Mech* 242:107451. <https://doi.org/10.1016/j.engfracmech.2020.107451>
- Gan Q, Xu J, Peng S, Yan F, Wang R, Cai G (2021) Effects of heating temperature on pore structure evolution of briquette coals. *Fuel* 296:120651. <https://doi.org/10.1016/j.fuel.2021.120651>
- Gao Y, Gao F, Dong G, Yan W, Yang X (2019) The mechanical properties and fractal characteristics of the coal under temperature-gas-confining pressure. *Therm Sci* 23:789–798. <https://doi.org/10.2298/TSCI180610094G>
- Gu J, Zhang W, Huang J, Du W, Wang Q, Hao H (2017) Reducing fluid channelling risk after hydraulic fracturing using mud cake to agglomerated cake method in coalbed methane well. *Int J Oil Gas Coal Technol* 14(3):201–215. <https://doi.org/10.1504/IJOGCT.2017.10002914>
- Guo H, Sun Z, Ji M, Wu Y, Nian L (2022) An investigation on the impact of unloading rate on coal mechanical properties and energy evolution law. *Int J Environ Res Public Health* 19(8):45–46. <https://doi.org/10.3390/ijerph19084546>
- Hu S, Wang D, Li Y, Liu X, Zhou F, Wang M, He C, Yu B (2022) Thermo-hydro-mechanical coupling numerical simulation on mechanical heterogeneity of coal rock. *Geofluids* 2022:9410245. <https://doi.org/10.1155/2022/9410245>
- Hu Z, Sun J, Tang M (2018) An experimental study on the interaction law of the pore gas pressure and stress in gassy coals. *Tehnički Vjesnik* 25(4):1154–1161. <https://doi.org/10.17559/TV-20180805103717>
- Jia H, Hu Q, Fan B, Mao C, Zhang Q (2021) Causes for low CBM production of vertical wells and efficient development technology in Northern Zhengzhou Block in Qinshui Basin. *Coal Geol Explor* 49(2):34–42. <https://doi.org/10.3969/j.issn.1001-1986.2021.02.005>. (in Chinese)
- Jiang C, Duan M, Yin G, Wang J, Lu T, Xu J, Zhang D, Huang G (2017) Experimental study on seepage properties, AE characteristics and energy dissipation of coal under tiered cyclic loading. *Eng Geol* 221:114–123. <https://doi.org/10.1016/j.enggeo.2017.03.005>
- Jiang C, Li Z, Wang W, Wen Z, Duan M, Geng W (2021) Experimental investigation of the mechanical characteristics and energy dissipation of gas-containing coal under incremental tiered cyclic loading. *Geomech Geophys Geo-Energy Geo-Resour* 7(3):75. <https://doi.org/10.1007/s40948-021-00274-1>
- Kumar S, Tiwari G, Parameswaran V, Das A (2022) Rate-dependent mechanical behavior of jointed rock with an impersistent joint under different infill conditions. *J Rock Mech Geotech Eng* 14(5):1380–1393. <https://doi.org/10.1016/j.jrmge.2022.05.002>
- Laouafa F, Farret R, Vidal-Gilbert S, Kazmierczak JB (2016) Overview and modeling of mechanical and thermomechanical impact of underground coal gasification exploitation. *Mitig Adapt Strat Glob Change* 21(4):547–576. <https://doi.org/10.1007/s11027-014-9542-y>
- Li M, Cao J, Li W (2016) Stress and damage induced gas flow pattern and permeability variation of coal from Songzao Coalfield in Southwest China. *Energies* 9(5):351. <https://doi.org/10.3390/en9050351>
- Li H, Lau H, Huang S (2018a) China's coalbed methane development: a review of the challenges and opportunities in subsurface and surface engineering. *J Petrol Sci Eng* 166:621–635. <https://doi.org/10.1016/j.petrol.2018.03.047>
- Li Q, Liang Y, Zou Q (2018b) Seepage and damage evolution characteristics of gas-bearing coal under different cyclic loading–unloading stress paths. *Processes* 6(10):190. <https://doi.org/10.3390/pr6100190>

- Li X, Zhang J, Li C, Li B, Zhao H, Li R, Qi Q (2021a) Variation characteristics of coal-rock mechanical properties under varying temperature conditions for Shanxi Linfen coalbed methane well in China. *J Pet Explor Prod Technol* 11(7):2905–2915. <https://doi.org/10.1007/s13202-021-01186-2>
- Li X, Li H, Yang Z, Sun Z, Zhuang J, Song C, Wang X (2021b) Experimental study on triaxial unloading failure of deep composite coal-rock. *Adv Civ Eng* 2021:6687051. <https://doi.org/10.1155/2021/6687051>
- Liu S, Li X, Wang D, Wu M, Yin G, Li M (2019) Mechanical and acoustic emission characteristics of coal at temperature impact. *Nat Resour Res* 29(3):1755–1772. <https://doi.org/10.1007/s11053-019-09562-w>
- Liu A, Liu S (2022) Mechanical property alterations across coal matrix due to water-CO₂ treatments: a micro-to-nano scale experimental study. *Energy* 248:123575. <https://doi.org/10.1016/j.energy.2022.123575>
- Liu B, Wang J, He H, Vivek M, Li Y, Wang J, Zhao C (2020) Geochemistry of carboniferous coals from the Laoyagou Mine, Ningwu coalfield, Shanxi Province, Northern China: Emphasis on the enrichment of valuable elements. *Fuel* 279:118414. <https://doi.org/10.1016/j.fuel.2020.118414>
- Lu Z, Ju W, Gao F, Yi K (2022) Influence of loading rate on the failure characteristics of composite coal-rock specimens under quasi-static loading conditions. *Rock Mech Rock Eng* 55(2):909–921. <https://doi.org/10.1007/s00603-021-02699-2>
- Ma Q, Tan Y, Liu X, Zhao Z, Fan D, Purev L (2021) Experimental and numerical simulation of loading rate effects on failure and strain energy characteristics of coal-rock composite samples. *J Cent South Univ* 28(10):3207–3222. <https://doi.org/10.1007/s11771-021-4831-6>
- Mazaira A, Konicek P (2015) Intense rockburst impacts in deep underground construction and their prevention. *Can Geotech J* 52(10):1426–1439. <https://doi.org/10.1139/cgj-2014-0359>
- Miao S, Cai M, Guo Q, Huang Z (2016) Rock burst prediction based on in-situ stress and energy accumulation theory. *Int J Rock Mech Min Sci* 83:86–94. <https://doi.org/10.1016/j.ijrmmms.2016.01.001>
- Ouyang Z, Zhang G, Li Q, Lai X, Qin H, Zhao X, Zhou X (2020) Study on the rock burst tendentiousness of coal under different gas pressures. *Arab J Geosci* 13(1):1–13. <https://doi.org/10.1007/s12517-019-4991-y>
- Raziperchikolae S, Singh V, Kelley M (2020) The effect of Biot coefficient and elastic moduli stress-pore pressure dependency on poroelastic response to fluid injection: laboratory experiments and geomechanical modeling. *Greenh Gases Sci Technol* 10(5):980–998. <https://doi.org/10.1002/ghg.2019>
- Shen J, Zhan S, Karakus M, Zuo J (2021) Effects of flaw width on cracking behavior of single-flawed rock specimens. *Bull Eng Geol Environ* 80(2):1701–1711. <https://doi.org/10.1007/s10064-020-02029-w>
- Shen J, Shu Z, Cai M, Du S (2020) A shear strength model for anisotropic blocky rock masses with persistent joints. *Int J Rock Mech Min Sci* 134:104430. <https://doi.org/10.1016/j.ijrmmms.2020.104430>
- Souley M, Hoxha D, Homand F (1996) Distinct element modelling of an underground excavation using a continuum damage model. *Int J Rock Mech Min Sci Geomech Abstr* 35(4–5):442–443. [https://doi.org/10.1016/S0148-9062\(98\)00042-4](https://doi.org/10.1016/S0148-9062(98)00042-4)
- Su C, Qiu J, Wu Q, Weng L (2020) Effects of high temperature on the microstructure and mechanical behavior of hard coal. *Int J Min Sci Technol* 30(5):643–650. <https://doi.org/10.1016/j.ijmst.2020.05.021>
- Tang Z, Li Q, Yin H (2018) The influence of solute concentration and temperature of drilling fluids on wellbore failure in tight formation. *J Petrol Sci Eng* 160:276–284. <https://doi.org/10.1016/j.petrol.2017.10.053>
- Wang K, Du F (2019) Experimental investigation on mechanical behavior and permeability evolution in coal-rock combined body under unloading conditions. *Arab J Geosci* 12(14):422. <https://doi.org/10.1007/s12517-019-4582-y>
- Wang G, Guo Y, Wang P, Li W, Wu M, Sun L, Cao J, Du C (2020) A new experimental apparatus for sudden unloading of gas-bearing coal. *Bull Eng Geol Environ* 79(2):857–868. <https://doi.org/10.1007/s10064-019-01601-3>
- Wang J, Wang Q, Shi J, Li Z (2015) Distribution and enrichment mode of Li in the No. 11 coal seam from Pingshuo Mining District, Shanxi Province. *Energy Explor Exploit* 33(2):203–215. <https://doi.org/10.1260/0144-5987.33.2.203>
- Wang X, Wang E, Liu X, Zhou X (2021) Failure mechanism of fractured rock and associated acoustic behaviors under different loading rates. *Eng Fract Mech* 247:107674. <https://doi.org/10.1016/j.engfracmech.2021.107674>
- Wei H, Ma L, Wu J, Yu J, Li Z, Xu R (2022) Dynamic mechanical behavior of coral rock subjected to high strain rate loading. *Mar Geophys Res* 43(3):30. <https://doi.org/10.1007/s11001-022-09493-x>
- West RD, Markevicius G, Malhotra VM, Hofer S (2012) Variations in the mechanical behavior of Illinois bituminous coals. *Fuel* 98:213–217. <https://doi.org/10.1016/j.fuel.2012.03.042>
- Xie G, Yin Z, Wang L, Hu Z, Zhu C (2017) Effects of gas pressure on the failure characteristics of coal. *Rock Mech Rock Eng* 50(7):1711–1723. <https://doi.org/10.1007/s00603-017-1194-2>
- Xie H, Gao F, Ju Y (2015) Research and exploration of deep rock mechanics. *J Rock Mech Geotech Eng* 34:2161–2178. <https://doi.org/10.13722/j.cnki.jrme.2015.1369>. (In Chinese)
- Xin C, Wang K, Du F, Zhang X, Wang G, Liu Y (2018) Mechanical properties and permeability evolution of gas-bearing coal under phased variable speed loading and unloading. *Arab J Geosci* 11(23):747. <https://doi.org/10.1007/s12517-018-4117-y>
- Xue Y, Ranjith PG, Dang F, Liu J, Wang S, Xia T, Gao Y (2020) Analysis of deformation, permeability and energy evolution characteristics of coal mass around borehole after excavation. *Nat Resour Res* 29(5):3159–3177. <https://doi.org/10.1007/s11053-020-09644-0>
- Yang W, Lin B, Yan Q, Zhai C (2014) Stress redistribution of longwall mining stope and gas control of multi-layer coal seams. *Int J Rock Mech Min Sci* 72:8–15. <https://doi.org/10.1016/j.ijrmmms.2014.08.009>

- Yang Y, Chu J, Yan X (2007) Study on constitutive relationship of coal based on conventional triaxial compression test. *J Coal Sci Eng* 13(3):336–339
- Yin G, Li W, Jiang C, Li M, Li X, Liu H, Zhang Q (2013) Mechanical property and permeability of raw coal containing methane under unloading confining pressure. *Int J Min Sci Technol* 23(6):789–793. <https://doi.org/10.1016/j.ijmst.2013.10.002>
- Yin G, Li M, Wang J, Xu J, Li W (2015a) Mechanical behavior and permeability evolution of gas infiltrated coals during protective layer mining. *Int J Rock Mech Min Sci* 80:292–301. <https://doi.org/10.1016/j.ijrmms.2015.08.022>
- Yin G, Jiang C, Wang J, Xu J (2015b) Geomechanical and flow properties of coal from loading axial stress and unloading confining pressure tests. *Int J Rock Mech Min Sci* 76:155–161. <https://doi.org/10.1016/j.ijrmms.2015.03.019>
- Yin Z, Chen Z, Chang J, Hu Z, Ma H, Feng R (2019) Crack initiation characteristics of gas-containing coal under gas pressures. *Geofluids* 2019:1–12. <https://doi.org/10.1155/2019/5387907>
- Yin G, Li M, Li W, Jiang C, Cao J, Zhang Q (2012) Influence of gas pressure on mechanical and seepage characteristics of coal under unloading condition. *J China Coal Soc* 37(9):1499–1504. <https://doi.org/10.13225/j.cnki.jccs.2012.09.020>. (in Chinese)
- Zhang Q, Fan X, Liang Y, Li M, Li G, Ma T, Nie W (2017) Mechanical behavior and permeability evolution of reconstituted coal samples under various unloading confining pressures-implications for wellbore stability analysis. *Energies* 10(3):292. <https://doi.org/10.3390/en10030292>
- Zhang Q, Fan X, Chen P, Ma T, Zeng F (2020) Geomechanical behaviors of shale after water absorption considering the combined effect of anisotropy and hydration. *Eng Geol* 269:105547. <https://doi.org/10.1016/j.enggeo.2020.105547>
- Zhang B, Li X, Zhang D (2021a) Study on mechanical and permeability characteristics of containing gas coal-rock under conventional triaxial compression. *Geotech Geol Eng* 39(8):5775–5786. <https://doi.org/10.1007/S10706-021-01866-0>
- Zhang G, Ranjith PG, Li Z, Gao M, Ma Z (2021b) Long-term effects of CO₂-water-coal interactions on structural and mechanical changes of bituminous coal. *J Pet Sci Eng* 207:109093. <https://doi.org/10.1016/j.petrol.2021.109093>
- Zhang C, Cheng P, Ma Z, Ranjith PG, Zhou J (2021c) Comparison of fracturing unconventional gas reservoirs using CO₂ and water: an experimental study. *J Pet Sci Eng* 203:108598. <https://doi.org/10.1016/j.petrol.2021.108598>
- Zhang Q, Li X, Gao J, Jia S, Ye X (2022) Macro-and meso-damage evolution characteristics of coal using acoustic emission and keuence testing technique. *Nat Resour Res* 31(1):517–534. <https://doi.org/10.1007/s11053-021-10006-7>
- Zhong C, Zhang Z, Ranjith PG, Zhang C, Xue K (2022) The role of pore pressure on the mechanical behavior of coal under undrained cyclic triaxial loading. *Rock Mech Rock Eng* 55(3):1375–1392. <https://doi.org/10.1007/s00603-021-02705-7>
- Zhou C, Karakus M, Xu C, Shen J (2020) A new damage model accounting the effect of joint orientation for the jointed rock mass. *Arab J Geosci* 13(7):1–13. <https://doi.org/10.1007/s12517-020-5274-3>
- Zou Q, Liu H, Jiang Z, Wu X (2021) Gas flow laws in coal subjected to hydraulic slotting and a prediction model for its permeability-enhancing effect. *Energy Sources Part A Recovery Util Environ Effects* 2021:1936692. <https://doi.org/10.1080/15567036.2021.1936692>
- Zou Q, Zhang T, Ma T, Tian S, Jia X, Jiang Z (2022) Effect of water-based SiO₂ nanofluid on surface wettability of raw coal. *Energy* 254(Part A):124228. <https://doi.org/10.1016/j.energy.2022.124228>

Publisher's Note Springer Nature remains neutral with regard to jurisdictional claims in published maps and institutional affiliations.